RSC Advances

PAPER

View Article Online
View Journal | View Issue

Cite this: *RSC Adv.*, 2024, **14**, 30440

Selective synthesis of cyclic alcohols from cycloalkanes using nickel(II) complexes of tetradentate amidate ligands†

Anjana Rajeev,[a] Sethuraman Muthuramalingam[b] and Muniyandi Sankaralingam *[a]

Selective functionalisation of hydrocarbons using transition metal complexes has evoked significant research interest in industrial chemistry. However, selective oxidation of unactivated aliphatic C–H bonds is challenging because of the high bond dissociation energies. Herein, we report the synthesis, characterisation and catalytic activity of nickel(II) complexes ($[Ni(\mathbf{L1–L3})(OH_2)_2](ClO_4)_2$ (**1–3**)) of monoamidate tetradentate ligands [**L1**: 2-(bis(pyridin-2-ylmethyl)amino)-*N*-phenylacetamide, **L2**: 2-(bis(2-pyridin-2-ylmethyl)amino)-*N*-(naphthalen-1-yl)acetamide, **L3**: *N*-benzyl-2-(bis(pyridin-2-ylmethyl) amino)acetamide] in selective oxidation of cycloalkanes using *m*-CPBA as the oxidant. In cyclohexane oxidation, catalysts showed activity (TON) in the order **1** (654) > **2** (589) > **3** (359) with a high A/(K + L) ratio up to 23.6. Using catalyst **1**, the substrate scope of the reaction was broadened by including other cycloalkanes such as cyclopentane, cycloheptane, cyclooctane, adamantane and methylcyclohexane. Further, the Fenton-type reaction in the catalytic cycle was discarded based on the relatively high 3°/2° ratio of 8.6 in adamantane oxidation. Although the formation of chlorinated products during the reactions confirmed the contribution of the 3-chlorobenzoyloxy radical mechanism, the high alcohol selectivity obtained for the reactions indicated the participation of nickel-based oxidants in the oxidation process.

Received 18th July 2024
Accepted 24th August 2024

DOI: 10.1039/d4ra05222f

rsc.li/rsc-advances

1. Introduction

Modern catalytic approaches introduced a phenomenal change in synthetic and industrial chemistry by offering proficient and sustainable methods for synthesising organic molecules of paramount importance.[1,2] In this context, harnessing transition metal catalysts in functionalisation reactions has sparked increasing research interest.[3–5] The advent of transition metal-based catalysis opened up new possibilities for organic transformations that were once thought to be unattainable. For example, the oxidation of a hydrocarbon such as cyclohexane produces cyclohexanol and cyclohexanone, which are high-value-added compounds with versatile applications.[6] However, this oxidation is a strenuous task due to the high C–H bond dissociation energy of cyclohexane and requires multi-step procedures as well as rigorous reaction conditions.[6,7] Conversely, various catalysts, especially, 3d-metal molecular catalysts are known to mediate cyclohexane oxidation efficiently under mild reaction conditions in the presence of a suitable oxygen source.[4,8–21] The catalytic potential of nickel complexes in cyclohexane oxidation was first demonstrated using complex $[Ni(TPA)(OAc)(H_2O)](BPh_4)$ (**I**) (TPA = tris(2-pyridylmethyl) amine) and *meta*-chloroperbenzoic acid (*m*-CPBA).[11] Later, several notable attempts using nickel complexes with diverse ligands were reported, among which nickel(II) complexes of tetradentate ligands (**I–VI**) (Scheme 1) showed promising activity in terms of turnover number (TON) and alcohol selectivity (A/(K + L); A = cyclohexanol, K = cyclohexanone, L = caprolactone).[4,11–17] Also, pyridine is present as the donor moiety in most of these complexes and its replacement by phenolic or oxazoline groups has resulted in improved activity (catalysts **II** and **VI**).[12,16] Nevertheless, systematic tuning of ligands by introducing distinct donor moieties and evaluating the catalytic properties of corresponding complexes has been less examined in cyclohexane oxidation mediated by nickel(II) complexes. Moreover, ligands that can stabilise or facilitate the formation of reactive nickel oxygen species need to be synthesised for developing more selective and potential catalysts.

Intriguingly, amidate ligands are an exemplary choice for developing competent catalysts due to their ability to stabilise higher oxidation states of nickel, which is a key factor in governing the catalytic potential of many complexes.[22–27] For

[a]*Bioinspired & Biomimetic Inorganic Chemistry Lab, Department of Chemistry, National Institute of Technology Calicut, Kozhikode, Kerala 673601, India. E-mail: msankaralingam@nitc.ac.in; sankarjan06@gmail.com*

[b]*Institut de Química Computacional i Catalisi; (IQCC), Departament de Química, Universitat de Girona, Girona E-17003, Catalonia, Spain*

† Electronic supplementary information (ESI) available: Characterization of ligands and complexes are provided in Fig. S1–S9. The catalytic oxidation of adamantane and methylcyclohexane data are provided in Tables S1 and S2. CCDC 2371833 and 2371834. For ESI and crystallographic data in CIF or other electronic format see DOI: https://doi.org/10.1039/d4ra05222f

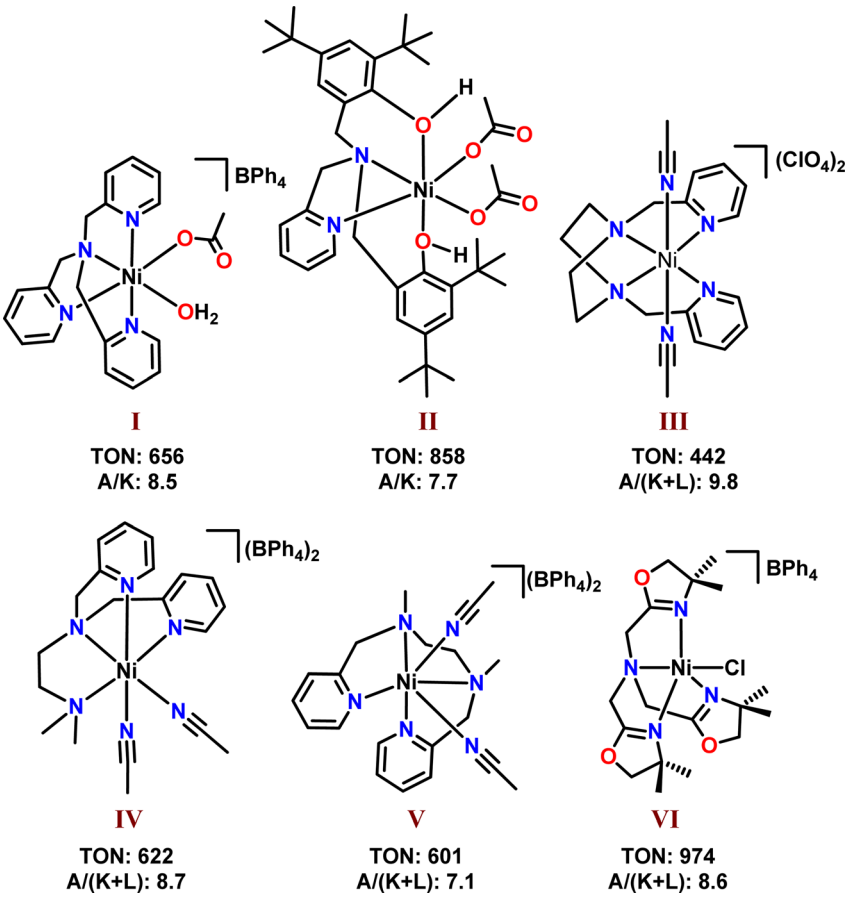

Scheme 1 Notable reported nickel(II) complexes of tetradentate ligands as the catalysts for cyclohexane oxidation.

instance, McDonald *et al.* and Company *et al.* have extensively worked on generating, characterising and exploring the reactivity of different high-valent nickel species supported by amidate ligands.[22–27] Notably, we recently reported that nickel(II) complexes with aminoquinoline-based monoamidate pincer ligands exhibit superior catalytic activity in the oxidation of cycloalkanes compared to other nickel catalysts containing tridentate ligands using *m*-CPBA as the oxidant.[28] The latest studies on the mechanism of cyclohexane oxidation by nickel(II) complexes confirm the involvement of the 3-chlorobenzoyloxy radical pathway and a partial contribution of nickel-based oxidant in the catalytic cycle.[29–31]

Also, it is noted that the steric factors of the catalysts play a pivotal role in the activity and therefore, it is essential to delve deeper into the impact of ligand choices in the catalytic performances of nickel(II) complexes. For this reason, we sought to develop nickel(II) complexes (**1–3**) containing monoamidate tetradentate ligands, [2-(bis(pyridin-2-ylmethyl)amino)-*N*-phenylacetamide (**L1**; [Ni(**L1**)(H_2O)$_2$](ClO_4)$_2$ (**1**)), 2-(bis(2-pyridin-2-ylmethyl)amino)-*N*-(naphthalen-1-yl)acetamide (**L2**; [Ni(**L2**)(H_2O)$_2$](ClO_4)$_2$ (**2**)), and *N*-benzyl-2-(bis(pyridin-2-ylmethyl)amino) acetamide (**L3**; [Ni(**L3**)(H_2O)$_2$](ClO_4)$_2$ (**3**))] and probed their catalytic potential in cycloalkane oxidation using *m*-CPBA as the oxidant. All the complexes catalyzed the oxidation of cyclohexane and produced cyclohexanol with excellent selectivity. High 3°/2° obtained in the oxidation substrates such as adamantane and methylcyclohexane ruled out the possibility of the hydroxyl radical mechanism in the oxidation reaction. In addition, the formation of chlorinated products during the oxidation of other cycloalkanes (cyclopentane, cycloheptane and cyclooctane) revealed the involvement of the free radical mechanism. However, higher selectivity achieved for the cyclic alcohols implies that the contribution of a metal-based oxidant cannot be discarded in the catalytic cycle.

2. Experimental sections

2.1. Materials

All reagents used to synthesise ligands and complexes were analytical grade and used as such except for *m*-CPBA. Aminomethyl pyridine (99%), diethyl ether (99%), *m*-CPBA (77%), hydrogen peroxide (30%) (H_2O_2), carbon tetrabromide (CBr_4) and acetonitrile (CH_3CN) HPLC grade were purchased from Merck. Aniline (99%), pyridine-2-carboxaldehyde (99%), sodium borohydride (98%), and nickel(II) perchlorate hexahydrate were procured from ThermoFisher Scientific. Chloroacetyl chloride (98%) and *tert*-butyl hydroperoxide (70%) (*t*-BuOOH) were purchased from Spectrochem. Triethylamine and naphthylamine were purchased from TCI Chemicals. Benzylamine was purchased from SRL India. Methanol, dichloromethane

(DCM), chloroform, and acetone were purchased from Qualigens. Methanol was distilled over magnesium turnings (10 equiv.) and iodine (1 equiv.). Acetone and dichloromethane were distilled using calcium chloride and calcium hydride, respectively. The *m*-CPBA was purified by dissolving 30 g in 200 mL of diethyl ether and washing with phosphate buffer (pH 7.4, 150 mL). The organic portions were collected by extraction and dried to obtain *m*-CPBA with >90% purity.

Caution note! As dried m-CPBA is shock-sensitive, suitable precautions should be taken when it is handled.

2.2. Physical measurements

^{1}H-NMR/^{13}C-NMR spectra of ligands were collected on Jeol 500 MHz spectrometer. UV-visible spectra of complexes were recorded in Agilent 8454 diode array spectrometer in acetonitrile at room temperature. The attenuated total reflection infrared (ATR-IR) spectra of samples were obtained using Jasco 4700 ATR-FTIR spectrometer at room temperature. Electrospray ionisation mass spectrometry (ESI-MS) data of the complexes were measured by Bruker Daltonics-esquire 6000. After catalysis, product analysis including identification and quantification was done using an Agilent 8860 GC series gas chromatograph equipped with an FID detector, HP-5 GC column (30 m × 0.32 mm × 0.25 μm). Post-reaction mixture of cyclohexane oxidation in the presence of CBr_4 was analysed using an Agilent 7820A gas chromatograph equipped with an HP-5 capillary column 30 m × 0.32 mm × 0.25 μm and a flame ionisation detector. High-resolution mass spectrometry (HRMS) data of the *m*-CBA adduct was recorded using Waters Synapt XS HRMS instrument.

2.3. Single crystal X-RD measurements

The X-ray intensity data were collected on a D8 QUEST ECO three-circle diffractometer system equipped with a Ceramic X-ray tube (Mo Kα, $\lambda = 0.71073$ Å) and a doubly curved silicon crystal Bruker Triumph monochromator. Single crystals were mounted using a fiber loop and optically centred. Multi-scan was used for the absorption correction. The structures were solved by direct methods with the program SHELXL-2019/1 (Sheldrick, 2019) and refined by full-matrix least-squares, based on F^2 method using the program SHELXL-2017/1 (Sheldrick, 2017).

2.4. Generation of steric maps

To calculate the steric map SambVca 2.1A web application was used which can be found at **https://www.aocdweb.com/OMtools/sambvca2.1/index.html**.[32] In the web user interface, the required complex was oriented in a Cartesian frame with a chosen point at the origin (Ni), a second point along the *z*-axis (coordinating nitrogens from the pyridine rings in the same axis) and a third point in the *xz* plane (one of the pyridine nitrogens in the *z*-direction). After alignment of the complex, nickel and acetonitrile or water molecules, that must be ignored from the steric map calculations were deleted, and the first coordination sphere around the metal was analysed.

2.5. Synthesis of ligands and complexes

Synthesis of all the ligands **L1–L3** was done in three steps by following/modifying the procedures in the literature and step 1 is the same for all the ligands.[33–37] Complexes were prepared by treating the required ligand with nickel(II) perchlorate hexahydrate in methanol at room temperature.

2.5.1. Synthesis of ligands L1–L3

*2.5.1.1. Synthesis of 2-(bis(pyridin-2-ylmethyl)amino)-N-phenylacetamide (**L1**).* Step 1: synthesis of bis(2-pyridylmethyl) amine: synthesis was done by following the procedure available in the literature.[33] Aminomethyl pyridine (0.514 mL, 5 mmol) was added to a methanolic solution of pyridine-2-carboxaldehyde (0.475 mL, 5 mmol) and stirred for 12 h. Afterwards, sodium borohydride (0.226 g, 6 mmol) was added to the reaction mixture under ice-cold conditions and stirred for another 12 h at room temperature. The crude reaction mixture was concentrated under reduced pressure and extracted with DCM (100 mL × 3). Organic fractions were collected, dried over sodium sulfate and concentrated to obtain a yellowish-brown oil. Yield: 0.95 g, 95%.

Step 2: synthesis of 2-chloro-*N*-phenylacetamide: synthesis was done by adapting the existing procedure in the literature.[34] Aniline (0.24 mL, 2.65 mmol) was dissolved in dry DCM under nitrogen atmosphere and stirred at ice-cold condition. To this, triethylamine (TEA, 0.154 mL, 1.1 mmol) in dry DCM was initially added and then chloroacetylchloride (0.35 mL, 4.42 mmol) in dry DCM was added dropwise. The resulting reaction mixture was allowed to stir for 1 h. After that, the crude reaction mixture was concentrated under reduced pressure and extracted with DCM (50 mL × 3). Organic fractions were collected and dried using sodium sulfate and concentrated to obtain the product as a white solid. Yield: 0.46 g, 92%.

Step 3: synthesis of 2-(bis(pyridin-2-ylmethyl)amino)-*N*-phenylacetamide (**L1**): synthesis was done by following the existing procedure in the literature.[34] A mixture of 2-chloro-*N*-phenylacetamide (0.25 g, 1.48 mmol), bis(2-pyridylmethyl)amine (0.29 g, 1.48 mmol), *N*,*N*-diisopropylethylamine (0.287 g, 2.22 mmol) and potassium iodide (245 mg) was degassed for 30 min. Then, the reaction mixture was refluxed and stirred for 12 h under nitrogen atmosphere. The solvent from the reaction solution was removed using a rotary evaporator to obtain a brown oil, which was purified using silica column chromatography using DCM-methanol (v/v = 40 : 1) as eluent. Yield: 0.43 g, 90%. ATR-IR, cm^{-1} (Fig. 2 (top)): 3329 cm^{-1} (N–H), 1671 cm^{-1} (C=O). ^{1}H NMR (500 MHz, $CDCl_3$) (Fig. S1†): (δ_H ppm) 10.86 (s, 1H), 8.60 (d, 2H), 7.76 (d, 2H), 7.62 (t, 2H), 7.34–7.29 (m, 4H), 7.16 (dd, 2H), 7.07 (t, 1H), 3.95 (s, 4H), 3.47 (s, 2H).

*2.5.1.2. Synthesis of 2-(bis(2-pyridin-2-ylmethyl)amino)-N-(naphthalen-1-yl)acetamide (**L2**).* Step 2: synthesis of 2-chloro-*N*-(naphthalen-1-yl)acetamide: synthesis was done by adapting the procedure in the literature.[35,36] Chloroacetylchloride (0.352 mL, 4.42 mmol) in dry DCM was slowly added to a mixture of 1-naphthylamine (0.53 g, 3.7 mmol) and triethylamine (0.62 mL, 4.42 mmol) in dry DCM at ice-cold condition under nitrogen atmosphere. Then, the reaction mixture was stirred for 20 h at room temperature. The solvent was evaporated under reduced

pressure and the residue was extracted with DCM (50 mL × 3). The organic fractions were collected and concentrated to get the product as white crystalline material. Yield: 0.6 g, 74%.

Step 3: synthesis of 2-(bis(2-pyridin-2-ylmethyl)amino)-*N*-(naphthalen-1-yl)acetamide (**L2**): synthesis was done by following the procedure in the literature.[36] A mixture of 2-chloro-*N*-(naphthalen-4-yl)acetamide (0.548 g, 2.50 mmol), bis(2-pyridylmethyl)amine (0.49 g, 2.45 mmol), *N*,*N*-diisopropylethylamine (0.325 g, 2.52 mmol) and potassium iodide (13 mg) was degassed for 30 min. Then, the reaction mixture was refluxed and stirred for 12 h under nitrogen atmosphere. The solvent from the reaction solution was removed using a rotary evaporator to obtain a brown oil, which was purified using silica column chromatography using chloroform-methanol (v/v = 30 : 1) as eluent. Yield: 0.66 g, 70%. ATR-IR, cm^{-1} (Fig. S2†(top)): 3275 cm^{-1} (N–H), 1682 cm^{-1} (C=O). ^{1}H NMR (500 MHz, $CDCl_3$) (Fig. S3†): (δ_H ppm) 11.09 (s, 1H), 8.49 (d, 2H), 8.41 (d, 1H), 8.11 (d,1H), 7.85 (d, 1H), 7.65–7.60 (m, 3H), 7.56–7.49 (m, 2H), 7.45 (t, 1H), 7.38 (d, 2H), 7.14 (dd, 2H), 4.07 (s, 4H), 3.60 (s, 2H).

2.5.1.3. Synthesis of N-benzyl-2-(bis(pyridin-2-ylmethyl) amino)acetamide (L3). Step 2: synthesis of *N*-benzyl-2-chloroacetamide: synthesis was done by modifying the procedure available in the literature.[34,37] Benzylamine (0.655 mL, 6 mmol) was dissolved in dry DCM at ice-cold condition under nitrogen atmoshphere. To this, triethylamine (0.35 mL, 2.5 mmol) in dry DCM was initially added followed by the drop-wise addition of chloroacetylchloride (0.796 mL, 10 mmol) in dry DCM. The reaction mixture was stirred in an ice bath for 1 h and an additional 2 h at room temperature. The solvent from the reaction solution was reduced under pressure and the residue was extracted with chloroform (100 mL × 3). The organic fractions were collected, dried over sodium sulfate, and concentrated to get the product as white crystalline material. Yield: 0.8 g, 72%.

Step 3: synthesis of *N*-benzyl-2-(bis(pyridin-2-ylmethyl) amino)acetamide (**L3**): synthesis was done by following the procedure used for synthesising **L1** and **L2**.[34,36] A mixture of *N*-benzyl-2-(bis(pyridin-2-ylmethyl)amino)acetamide (0.5 g, 2.72 mmol), bis(2-pyridylmethyl)amine (0.54 g, 2.72 mmol), *N*,*N*-diisopropylethylamine (0.53 g, 4.08 mmol) and potassium iodide (226 mg) was degassed for 30 min. Then, the reaction mixture was refluxed and stirred for 12 h under nitrogen atmosphere. The solvent from the reaction solution was removed using a rotary evaporator to obtain a brown oil, which was purified using silica column chromatography using DCM–methanol (v/v = 48 : 2) as eluent. Yield: 0.48 g, 51%. ATR-IR, cm^{-1} (Fig. S4† (top)): 3365 cm^{-1} (N–H), 1656 cm^{-1} (C=O). ^{1}H NMR (500 MHz, $CDCl_3$) (Fig. S5†): (δ_H ppm) 9.15 (s, 1H), 8.26 (d, 2H), 7.41 (t, 2H), 7.18 (d, 4H), 7.14–7.11 (m, 1H), 7.07 (d, 2H), 6.97 (dd, 2H), 4.35 (s, 2H), 3.73 (s, 4H), 3.28 (s, 2H). ^{13}C NMR (125 MHz, $CDCl_3$) (Fig. S6†): (δ_C ppm) 171.32, 157.95, 149.29, 138.47, 136.50, 128.45, 127.92, 127.10, 123.23, 122.39, 60.53, 58.10, 43.26.

2.5.2. Synthesis of nickel(II) complexes (1–3). Nickel(II) perchlorate hexahydrate (0.183 g, 0.5 mmol) was taken in a vial and dissolved in distilled methanol. To this, a methanolic solution of the ligand (**L1–L3**) (0.5 mmol) was added dropwise. The resulting solution was stirred for 1 h to complete the complex formation. The solvent was removed under reduced pressure to obtain a blue residue, which was washed with cold diethyl ether several times and dried to obtain the complex (**1–3**) as a blue powder.

$[Ni(\mathbf{L1})(H_2O)_2](ClO_4)_2$ (**1**): yield = 75%. ATR-IR, cm^{-1} (Fig. 2 (bottom)): 3343 cm^{-1} (N–H), 1649 cm^{-1} (C=O), 1055 cm^{-1}, 963 cm^{-1}, 617 cm^{-1} (ClO_4^-). ESI-MS m/z = 489.1 $\{[Ni(\mathbf{L1})]^{2+} + ClO_4^-\}^+$ (calcd. = 489.05) (Fig. S7†).

$[Ni(\mathbf{L2})(H_2O)_2](ClO_4)_2$ (**2**): yield = 84%. ATR-IR, cm^{-1} (Fig. S2† (bottom)): 3245 cm^{-1} (N–H), 1643 cm^{-1} (C=O), 1055 cm^{-1}, 972 cm^{-1}, 626 cm^{-1} (ClO_4^-). ESI-MS m/z = 539.1 $\{[Ni(\mathbf{L2})]^{2+} + ClO_4^-\}^+$ (calcd. = 539.06) (Fig. S8†). Single crystals of $[Ni(\mathbf{L2})(CH_3CN)_2](ClO_4)_2$ (**2a**) suitable for X-ray analysis were obtained in the diffusion method, where an acetonitrile solution of **2** in a vial was kept in another vial filled with diethyl ether for 1–2 days.

$[Ni(\mathbf{L3})(H_2O)_2](ClO_4)_2$ (**3**): yield = 60%. ATR-IR, cm^{-1} (Fig. S4† (bottom)): 3369 cm^{-1} (N–H), 1641 cm^{-1} (C=O), 1055 cm^{-1}, 963 cm^{-1}, 621 cm^{-1} (ClO_4^-). ESI-MS m/z = 503.1 $\{[Ni(\mathbf{L3})]^{2+} + ClO_4^-\}^+$ (calcd. = 503.06) (Fig. S9†). Single crystals of $[Ni(\mathbf{L3})(H_2O)(CH_3CN)](ClO_4)_2$ (**3a**) suitable for X-ray analysis were grown in the diffusion method, where a methanol–acetonitrile (v/v = 1 : 1) solution of **3** in a vial was kept in another vial filled with diethyl ether for 1–2 days.

2.6. Catalytic oxidation of cycloalkanes

2.6.1. Catalytic oxidation of cyclohexane. The catalytic oxidation of cyclohexane was performed in a DCM : MeCN mixture (v/v = 3 : 1) at 60 °C under nitrogen atmosphere for 2 h. Initially, the nickel catalyst (**1–3**) (0.15 mM) was taken in a reaction tube in a DCM : MeCN mixture (3 : 1 v/v) and cyclohexane (2.8 M) was added to it. Further, the oxidant *m*-CPBA (0.35 M) was added using a syringe under nitrogen atmosphere and the reaction mixture was stirred for 2 h at 60 °C. Then, the reaction mixture was cooled down to room temperature and internal standard (bromobenzene) was added to the mixture. It was then passed through a silica plug and eluted with diethyl ether. The products were identified using an Agilent 8860 GC series gas chromatograph equipped with an FID detector, HP-5 GC column (30 m × 0.32 mm × 0.25 μm). Product quantification was done using calibration curves of authentic samples obtained by following the temperature program with a split ratio of 25 : 1, inlet temperature = 130 °C, initial temperature = 40 °C, heating rate = 0.1 °C min^{-1} to 42 °C, 8 °C min^{-1} to 190 °C (hold 1 min). FID temperature = 280 °C.[28]

2.6.2. Catalytic oxidation of other cycloalkanes. The catalytic oxidation of other cycloalkanes (2.8 M: cyclopentane, cycloheptane, cyclooctane and methylcyclohexane) was carried out using the nickel catalyst **1** (0.15 mM) in a DCM : MeCN mixture (v/v = 3 : 1) at 60 °C under nitrogen atmosphere for 2 h. Further, the oxidant *m*-CPBA (0.35 M) was added dropwise using a syringe. Then, the reaction mixture was cooled down to room temperature and internal standard (bromobenzene) was added to it. It was then passed through a silica plug and eluted with diethyl ether. The products were identified using an Agilent

8860 GC series gas chromatograph equipped with an FID detector, HP-5 GC column (30 m × 0.32 mm × 0.25 μm) and quantified using calibration curves of authentic samples obtained by following the temperature program with a split ratio of 25 : 1, inlet temperature = 130 °C, initial temperature = 40 °C, heating rate = 0.1 °C min^{-1} to 42 °C, 8 °C min^{-1} to 190 °C (hold 1 min). FID temperature = 280 °C.[28]

2.6.3. Catalytic oxidation of adamantane. The catalytic oxidation of adamantane was carried out in a DCM : MeCN mixture (v/v = 3 : 1) at 60 °C under nitrogen atmosphere for 2 h. Firstly, the nickel catalyst (0.15 mM) was taken in a reaction tube containing the solvent followed by the addition of adamantane (0.27 M). Further, the oxidant *m*-CPBA (0.18 M) was added dropwise using a syringe under nitrogen atmosphere and the reaction mixture was stirred for 2 h at 60 °C. Then, the reaction mixture was cooled down to room temperature and internal standard (bromobenzene) was added to it. It was then passed through a silica plug and eluted with diethyl ether. The products were identified using an Agilent 8860 GC series gas chromatograph equipped with an FID detector, HP-5 GC column (30 m × 0.32 mm × 0.25 μm) and quantified using calibration curves of authentic samples obtained by following the temperature program with a split ratio of 25 : 1: inlet temperature = 130 °C, initial temperature = 60 °C, heating rate = 10 °C min^{-1} to 130 °C, then to 135 °C with a heating rate = 0.5 °C min^{-1} and finally to 220 °C at a heating rate = 20 °C min^{-1}, FID temperature = 280 °C.[28]

2.6.4. Cyclohexane oxidation in the presence of CBr_4. Catalyst **1** (0.15 mM) was taken in a reaction tube in a DCM : MeCN mixture (3 : 1 v/v) and cyclohexane (2.8 M) was added to it. Then, *m*-CPBA (0.35 M) was added using a syringe under nitrogen atmosphere followed by the addition of CBr_4 (0.35 M). The reaction mixture was stirred for 2 h at 60 °C. After that, the reaction mixture was cooled to room temperature and passed through a silica plug and eluted with diethyl ether. The mixture was analysed using an Agilent 7820A gas chromatograph equipped with an HP-5 capillary column 30 m × 0.32 mm × 0.25 μm and a flame ionisation detector.

3. Results and discussion

3.1. Synthesis of ligands and complexes

The ligands **L1–L3** (Scheme 2) were synthesised by adapting the procedures available in the literature and involved the dehydrohalogenation reaction between bis(2-pyridylmethyl)amine and the required acetamide precursor (Fig. S1–S6†).[33–37]

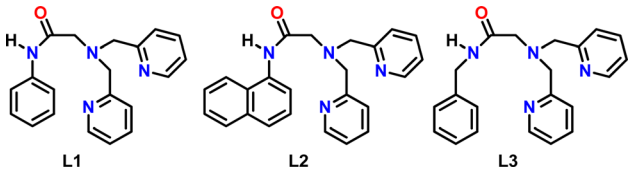

Scheme 2 Tetradentate ligands employed in this study.

The corresponding nickel(II) complexes (**1–3**) were prepared by reacting the ligands with nickel(II) perchlorate hexahydrate in distilled methanol. All the complexes were isolated as blue powder with good yields. Synthesised ligands and complexes were characterised with an array of advanced analytical techniques such as ^{1}H NMR, ATR-IR and UV-vis spectroscopies, ESI-MS and single crystal XRD. Based on these analyses, complexes were formulated as $[Ni(\mathbf{L1})(H_2O)_2](ClO_4)_2$ (**1**), $[Ni(\mathbf{L2})(H_2O)_2](ClO_4)_2$ (**2**), $[Ni(\mathbf{L3})(H_2O)_2](ClO_4)_2$ (**3**).

3.2. Characterisation of complexes

3.2.1 Electronic spectra. The electronic absorption spectra of complexes **1–3** were recorded in acetonitrile at room temperature and the data are summarised in Table 1. All the complexes showed typical UV-vis spectral patterns of nickel(II) complexes having octahedral geometry in the solution state with two broad absorption bands (Fig. 1).[18–20] With the help of the Tanabe–Sugano diagram, the high energy band in the range 548–553 nm is assigned to $^3A_{2g}(F) \rightarrow {}^3T_{1g}(F)$ (ν_2) transition and

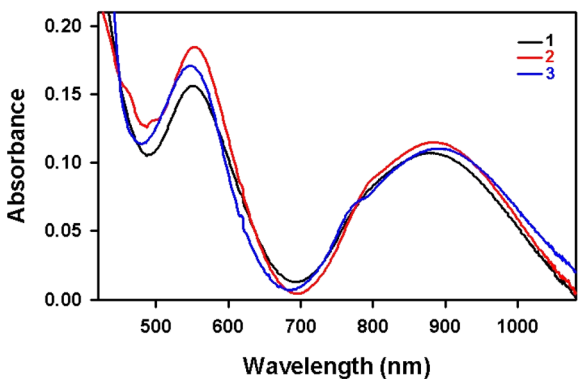

Fig. 1 UV-vis absorption spectra of complexes **1–3** (10 × 10^{-3} M) recorded in acetonitrile at room temperature.

Table 1 UV-vis spectral data (λ_{max} in nm; ε in M^{-1} cm^{-1} in parenthesis) of nickel(II) complexes **1–3** (10 mM) in acetonitrile at room temperature

	$^3A_{2g} \rightarrow {}^3T_{1g}(P)$ (ν_3)					
Complex	Found	calcd[a] (nm)	$^3A_{2g} \rightarrow {}^3T_{1g}(F)$ (ν_2) (nm)	$^3A_{2g} \rightarrow {}^3T_{2g}(F)$($\nu_1$) (nm)	B' (cm^{-1})	[a]β
1	–	343	551 (16)	880 (11)	879	0.813
2	–	345	553 (18)	885 (12)	876	0.811
3	–	326	548 (17)	893 (11)	1018	0.942

[a] Calculated by solving the quadratic equation and using B as 1080 cm^{-1}.

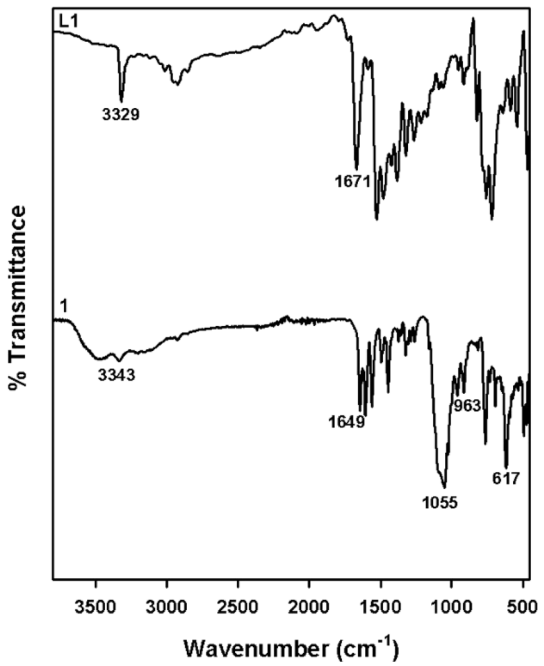

Fig. 2 ATR-IR spectra of ligand **L1** (top) and complex **1** (bottom).

the low energy broad band in the range 880–893 nm is assigned to $^3A_{2g}(F) \rightarrow {}^3T_{2g}(F)$ (ν_1).

In addition, a shoulder peak around 762–799 nm was also observed due to the spin-forbidden transition $^3A_{2g}(F) \rightarrow {}^1E_{1g}(D)$. The band corresponding to $^3A_{2g}(F) \rightarrow {}^3T_{1g}(P)$ (ν_3) transition was not observed experimentally probably due to the overlapping with the ligand-based high-energy transitions. However, using λ(nm) values of ν_1 and ν_2 transitions, ν_3 λ(nm) has been calculated for all the complexes (**1**, 343 nm; **2**, 345 nm; **3**, 326 nm, Table 1).

3.2.2 Vibrational spectra. To understand the vibrational properties of ligands and complexes ATR-IR spectroscopy was used. The comparison of ATR-IR spectra of ligands and complexes revealed that the amide nitrogen of ligand is not coordinating with the nickel(II) centre, instead the amide carbonyl oxygen is coordinating (Fig. 2, S2 and S4†). For example, ATR-IR spectra of all the ligands exhibited amide N–H stretching frequency in the range 3275–3365 cm^{-1} and similar peaks were observed in corresponding nickel(II) complexes in the range 3245–3369 cm^{-1}. This finding indicates that the deprotonation of amide nitrogen did not occur during the complex formation (while using TEA). Also, the presence of C=O stretching frequency in all the ligands (1656–1682 cm^{-1}) and respective complexes (1641–1649 cm^{-1}) implies that the C=O group of the ligands remains intact during complex formation. Moreover, all the complexes showed a broad intense peak at 1055 cm^{-1}, a sharp peak around 617–621 cm^{-1} and a weaker absorption peak around 963–972 cm^{-1}, which can be ascribed to the presence of uncoordinated ClO_4^- ions.[33,38,39]

3.2.3 Electrospray ionisation mass spectrometry (ESI-MS). ESI-MS of all the complexes in the positive ion mode was recorded in acetonitrile (Fig. S7–S9†). Complexes **1–3** showed a similar molecular ion peak in the form $\{[Ni(L)]^{2+} + ClO_4^-\}^+$, at $m/z = 489.1$ (for **1**; calcd. $m/z = 489.05$), $m/z = 539.1$ (for **2**; calcd. $m/z = 539.06$), and $m/z = 503.1$ (for **3**; calcd. $m/z = 503.06$) due to the removal of one of the uncoordinated perchlorate anions from the complexes. Besides, an additional peak was observed in the mass spectra of **2** corresponding to $\{[Ni(\mathbf{L2})-H]\}^+$.

3.2.4 Single-crystal XRD analysis. For the X-ray analysis, single crystals of $[Ni(\mathbf{L2})(CH_3CN)_2](ClO_4)_2$ (**2a**) and $[Ni(\mathbf{L3})(H_2O)(CH_3CN)](ClO_4)_2$ (**3a**) were obtained using vapour diffusion approach by dissolving $[Ni(\mathbf{L2})(H_2O)_2](ClO_4)_2$ (**2**) or $[Ni(\mathbf{L3})(H_2O)_2](ClO_4)_2$ (**3**) in a small vial containing acetonitrile/acetonitrile–methanol mixture and placing in a larger vial partially filled with diethyl ether. The ORTEP diagrams of **2a** and **3a** are shown in Fig. 3. The selected bond lengths and bond angles of **2a** and **3a** are summarised in Table 2 and their crystallographic data is provided in Table 3.

It is noteworthy that, unlike several amidate ligands, the amide nitrogen in **L2** and **L3** did not undergo deprotonation (even in the presence of TEA) during complex formation to coordinate with the nickel(II) centre, instead, the carbonyl oxygen participates in the coordination in both **2a** and **3a**.[28,40] A similar coordination behaviour was observed in the crystal structure of a zinc complex of **L2**.[36] Nickel(II) centre in both complexes resides in a distorted octahedral environment coordinated with three nitrogen atoms and one carbonyl oxygen atom of the respective ligand along with either two acetonitrile molecules (**2a**) or one acetonitrile molecule and a water molecule (**3a**). The acetonitrile molecules are coordinated during the crystallisation process. Bond angles of **2a** and **3a** fall in the

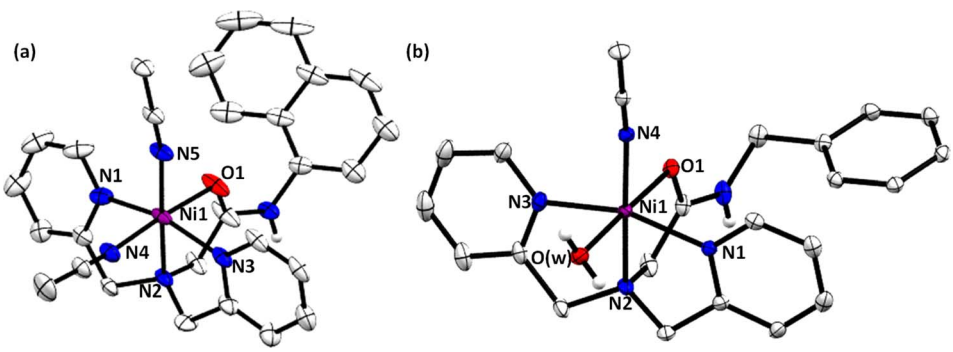

Fig. 3 ORTEP diagrams of the cationic part of complexes (a) **2a** and (b) **3a** with labelling schemes. Displacement ellipsoids are shown at 30% probability level. Hydrogen atoms (except from the amide group and water molecule) are omitted for clarity.

Table 2 Selected bond lengths [Å] and bond angles [°] for **2a** and **3a**

2a		**3a**	
Bond lengths [Å]			
Ni1–N5	2.028(3)	Ni1–N4	2.042(2)
Ni1–N4	2.089(4)	Ni1–N3	2.079(2)
Ni1–N3	2.075(4)	Ni1–N2	2.090(2)
Ni1–N2	2.090(3)	Ni1–N1	2.081(2)
Ni1–N1	2.057(4)	Ni1–O1	2.0649(19)
Ni1–O1	2.065(3)	Ni1–O(w)	2.072(2)
Bond angles [°]			
N5–Ni1–N4	90.76(12)	N4–Ni1–N3	100.01(10)
N5–Ni1–N3	97.49(14)	N4–Ni1–N2	177.00(10)
N5–Ni1–N2	174.26(13)	N4–Ni1–N1	99.06(9)
N5–Ni1–N1	100.70(14)	N3–Ni1–N2	79.77(9)
N4–Ni1–N2	94.39(12)	N3–Ni1–N1	160.80(9)
N3–Ni1–N4	90.03(13)	N1–Ni1–N2	81.30(9)
N3–Ni1–N2	80.02(12)	N4–Ni1–O1	93.17(8)
N3–Ni1–N1	161.81(12)	N3–Ni1–O1	94.44(8)
N1–Ni1–N4	89.81(13)	N2–Ni1–O1	83.88(9)
N1–Ni1–N2	81.86(12)	N1–Ni1–O1	86.69(8)
N5–Ni1–O1	92.10(11)	N4–Ni1–O(w)	88.51(9)
N4–Ni1–O1	176.28(13)	N3–Ni1–O(w)	85.77(9)
N3–Ni1–O1	91.95(14)	N2–Ni1–O(w)	94.45(10)
N2–Ni1–O1	82.86(11)	N1–Ni1–O(w)	92.53(9)
N1–Ni1–O1	87.31(14)	O1–Ni1–O(w)	178.24(9)

range 79.77(9)–100.70(14) and 160.80(9)–178.24(9), which deviate significantly from the ideal octahedral bond angles of 90° and 180°.

3.3. Oxidation of cycloalkanes

3.3.1. Oxidation of cyclohexane. The catalytic activity of complexes **1–3** toward oxidation of cycloalkanes was probed using cyclohexane as the model substrate using various oxidants such as O_2, H_2O_2, *t*-BuOOH and *m*-CPBA in DCM : MeCN (v/v = 3 : 1) mixture at 60 °C for 2 hours. However, *m*-CPBA was found to be the only suitable oxidant for the reaction (Fig. S10†) and afforded cyclohexanol (A) as the major product and cyclohexanone (K) along with caprolactone (L; formed due to the Baeyer–Villiger oxidation of K) as the minor products. In addition, chlorobenzene (PhCl; formed due to the dissociation of *m*-CPBA or *m*-CPBA adduct) and chlorocyclohexane (Cy^6Cl; produced by the chlorine atom abstraction of cyclohexyl radical ($Cy^{6\bullet}$) from the solvent DCM molecule) were also identified in the reaction mixture (Fig. S10†). The TON of oxidised products reported here is the average of three determinations, and it is calculated by taking the ratio of the number of mmol of formed product to the number of mmol of catalyst used. The catalytic activity was notably affected by the catalyst loading, oxidant concentration, temperature as well as time, and thus, the reaction conditions were optimised using catalyst **1** by tuning these parameters and the results are summarised in Table 4.

The effect of catalyst loading was studied using different catalyst concentrations (0.1–0.3 mM, Table 4, entries 1–5). Even though the achieved total TON was the highest (742) when 0.1 mM (Table 4, entry 1) of **1** was used, the obtained alcohol

Table 3 Crystallographic data of **2a** and **3a**

	2a	**3a**
Empirical formula	$C_{28}H_{28}Cl_2N_6NiO_9$	$C_{23}H_{27}Cl_2N_5NiO_{10}$
Formula weight (g mol^{-1})	722.17	663.10
Temperature (K)	100(2)	100(2)
Wavelength/(Å)	0.71073	0.71073
Crystal size (mm)	0.140 × 0.140 × 0.200	0.100 × 0.130 × 0.240
Crystal habit	Violet prism	Blue prism
Crystal system	Triclinic	Monoclinic
Space group	*P* -1	*P*1 $2_1/c$1
a (Å)	10.8951(6)	17.786(3)
b (Å)	12.6583(7)	7.4291(13)
c (Å)	12.8328(7)	21.345(4)
α (°)	87.684(2)	90
β (°)	77.714(2)	101.411(5)
γ (°)	72.944(2)	90
V (Å^3)	1652.77(16)	2764.6(8)
Z	2	4
ρ_{cald} (g cm^{-3})	1.451	1.593
ε (mm^{-1})	0.808	0.959
F(000)	744	1368
θ (min, max) (°)	2.31, 27.55	2.98, 27.57
Reflections collected	52 485	97 866
Independent reflections, *R* (int)	7553, 0.0184	6383, 0.0822
Max. and min. Transmission	0.8950 and 0.8550	0.9100 and 0.8020
Data/restraints/parameters	7553/13/555	6383/12/403
Goodness-of-fit on F^2	1.043	1.034
R1, wR_2 ($I > 2\sigma(I)$)[a]	0.0706, 0.2081	0.0429, 0.0942
R1, wR_2 (all data)	0.0761, 0.2147	0.0633, 0.1045

[a] $R_1 = [\Sigma(||F_o| - |F_c||)/\Sigma|F_o|]$; w$R2 = \{[\Sigma(w(F_o^2 - F_c^2)^2)/\Sigma(wF_o^4)]^{1/2}\}$.

Table 4 Effect of catalyst loading, oxidant concentration, temperature and time in cyclohexane oxidation using **1**[a]

Entry	Cat. conc.[b] (mM)	Cy^6Cl (TON)	A (TON)	K (TON)	L (TON)	Total TON[f]	PhCl (TON)	A/(K + L)
1	0.1	172	528	16	26	742	951	12.6
2	0.15	136	497	10	11	654	878	23.6
3	0.2	90	348	6	8	452	621	24.8
4	0.25	63	356	5	10	434	441	23.7
5	0.3	83	197	4	5	289	408	21.8
	Oxidant[c] (M)							
6	0.05	13	61	2	—	76	159	30.5
7	0.15	73	150	5	—	228	397	30.0
8	0.25	68	398	8	6	480	489	28.4
9	0.35	136	497	10	11	654	878	23.6
10	0.45	150	533	5	35	723	930	13.3
	Temp.[d] (°C)							
11	25	—	—	—	—	—	60	—
12	40	26	240	5	6	277	125	21.8
13	50	37	355	9	7	408	322	22.1
14	60	136	497	10	11	654	878	23.6
15	80	135	524	11	15	685	918	20.1
16	100	153	538	16	17	724	1107	16.3
	Time[e] (h)							
17	0.5	15	99	4	—	118	270	24.7
18	1.0	28	167	6	1	202	374	23.8
19	1.5	46	260	6	5	317	406	23.6
20	2.0	136	497	10	11	654	878	23.6
21	2.5	134	520	10	12	676	890	23.6
22	5	128	416	9	12	565	856	19.8
23	10	104	407	8	14	533	739	18.5
24	24	61	356	2	44	463	622	7.7

[a] Cy^6Cl = chlorocyclohexane, A = cyclohexanol, K = cyclohexanone, L = caprolactone, PhCl = chlorobenzene. [b] Reaction conditions: cyclohexane (2.8 M), oxidant (0.35 M), catalyst in DCM : MeCN solvent mixture (v/v = 3 : 1), 60 °C, 2 h under N_2. [c] Reaction conditions: cyclohexane (2.8 M), catalyst (0.15 mM) in DCM : MeCN solvent mixture (v/v = 3 : 1), 60 °C, 2 h under N_2. [d] Reaction conditions: cyclohexane (2.8 M), oxidant (0.35 M), catalyst (0.15 mM) in DCM : MeCN solvent mixture (v/v = 3 : 1), 2 h under N_2. [e] Reaction conditions: cyclohexane (2.8 M), oxidant (0.35 M), catalyst (0.15 mM) in DCM : MeCN solvent mixture (v/v = 3 : 1), 60 °C under N_2. [f] TON = number of mmol of product/number of mmol of catalyst. The TON is the average of three determinations.

selectivity (A/(K + L) = 12.6) was the lowest. Upon using 0.15 mM of catalyst, a double-fold increment in the alcohol selectivity (23.6) was noted with a total TON of 654 (Table 4, entry 2). As the catalyst concentration increased, the obtained total TON decreased by maintaining the alcohol selectivity (Table 4, entries 3–5). Therefore, the optimum catalyst loading was selected as 0.15 mM. Then, the reactions were performed under different oxidant concentrations (0.05–0.45 M) and evaluated the catalytic activity (Table 4, entries 6–10). When lower oxidant concentrations were used, the total TON obtained was poor, but, excellent alcohol selectivity was observed (Table 4, entries 6 and 7). With the increment in the amount of oxidant used, an enhancement in the total TON (480–723) and a drop in the A/(K + L) ratio (28.4–13.3) were noted (Table 4, entries 8–10). Based on the results, a high total TON (654) with a good A/(K + L) ratio (23.6) was achieved using 0.35 M of *m*-CPBA and it was taken as the optimum oxidant concentration (Table 4, entry 9). Further, the temperature effect on the catalytic activity was monitored by performing the reaction at different temperatures (25–100 °C; Table 4, entries 11–16). The reaction at 25 °C did not afford any oxidised products, rather a small amount of chlorobenzene (PhCl) was formed. A gradual increase in the total TON (277–724) was seen when the reaction temperature was changed with in the range of 40 °C to 100 °C. However, high temperatures favoured overoxidation as well as Baeyer–Villiger oxidation and produced more amount of K and L. This, in turn, reduced alcohol selectivity at high temperatures and thus 60 °C was chosen as the suitable temperature for the reaction. In addition, the effect of reaction time was also evaluated by carrying out the reactions for various time durations (Table 4, entries 17–24). Up to 2.5 h, an improvement in the total TON was noted with good alcohol selectivity. In contrast, keeping the reaction for 5, 10 or 24 h led to decreased activity, which could be due to the evaporation of solvent or volatile oxidised products over time. The difference in the catalytic activity was only marginal when the reaction time was 2 or 2.5 h and thus the optimum time for the reaction was selected as 2 h. Under optimised conditions, a control experiment was performed without using any catalyst and the oxidised products were formed in trace amounts (Table 5, entry 1). On the other hand, using catalysts **1–3**, the reaction progressed very well and afforded A, K and L along with Cy^6Cl and PhCl in moderate yield (15.4–28.0%). The catalytic

Table 5 Catalytic cyclohexane oxidation using **1–3**[a]

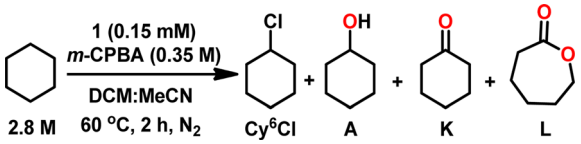

Entry	Catalyst[b]	Cy^6Cl (TON)	A (TON)	K (TON)	L (TON)	Total TON[c]	PhCl (TON)	A/(K + L)	Yield[d] (%)
1	None	25	52	9	—	86[e]	59	5.7	4
2	**1**	136	497	10	11	654	878	23.6	28.0
3	**2**	96	472	9	12	589	782	22.4	25.2
4	**3**	65	275	8	11	359	508	14.4	15.4
5	**1**	48	62	10	23	143	223	1.8	6.1

[a] Cy^6Cl = chlorocyclohexane, A = cyclohexanol, K = cyclohexanone, L = caprolactone, PhCl = chlorobenzene. [b] Reaction conditions: cyclohexane (2.8 M), oxidant (0.35 M), catalyst (0.15 mM) in DCM : MeCN solvent mixture (v/v = 3 : 1), 60 °C, 2 h under N_2. [c] TON = number of mmol of product/number of mmol of catalyst. The TON is the average of three determinations. [d] Yield based on *m*-CPBA. [e] Values based on 0.15 mM virtual nickel catalyst.

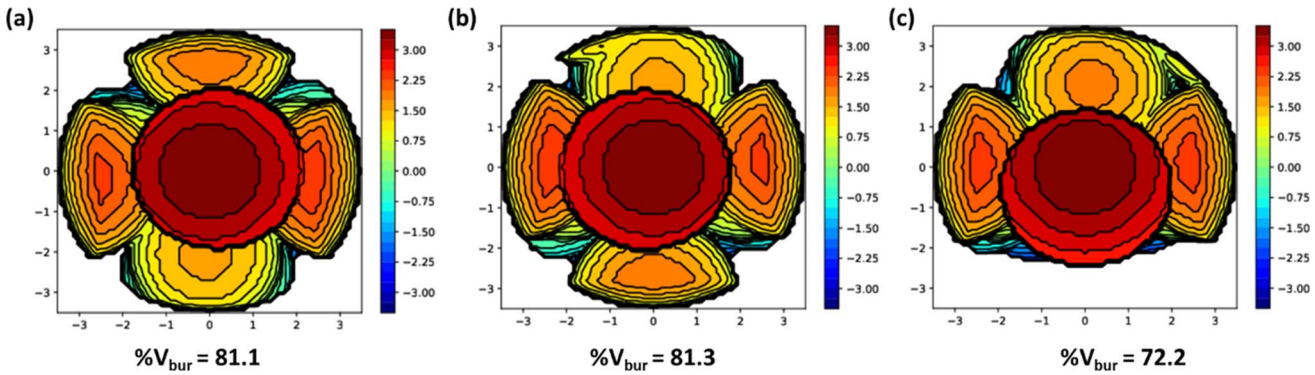

Fig. 4 Steric maps of **1** (a), **2** (b) and **3** (c) with % V_{bur} generated using SambVca 2.1 web application.

activity was in the order **1** > **2** > **3** in terms of total TON as well as A/(K + L) ratio (Table 5, entries 2–4).

The catalytic activity was majorly influenced by the steric factors of the ligands. The *m*-CPBA adduct formation with the catalyst or facile approach of the substrate towards the reactive species is favoured in a less steric-hindering environment. The bis(2-pyridylmethyl)amine unit is commonly present in all the complexes and imparts the same steric hindrance. On the other hand, monocyclic aniline donor moiety in complex **1** provides less steric hindrance than dicyclic naphthyl amine moiety in complex **2** and this could be attributed to the enhanced activity of **1** over **2**. Similarly, complex **3** containing monocyclic benzylamine moiety is expected to show more catalytic activity than complex **2**. Nevertheless, even with the lowest steric hindrance calculated for **3** (% V_{bur} = 72.2) using the SambVca 2.1 web application, it was found to be the least active catalyst (Fig. 4). This is possibly due to the rapid free rotation of the benzylic CH_2 group in **3**, that can hamper the easy access of *m*-CPBA or substrate to the nickel centre and decrease the catalytic activity. Also, the present catalysts have a higher % V_{bur} (72.2–81.3) than our recently reported aminoquinoline-based pincer nickel(II) catalysts (% V_{bur} = 57.7–66.0), which correlates with the greater activity observed for the latter set of complexes.[28]

Moreover, compared to previously reported tetradentate nickel complexes (Scheme 1 and Table 6), the total TON and overall yield were lower when catalysts **1–3** were used.[4] Despite that, remarkable improvement in the A/(K + L) ratio was

Table 6 Catalytic data of previously reported nickel(II) complexes of tetradentate ligands (selected examples) in cyclohexane oxidation using *m*-CPBA as the oxidant along with **1–3**

Catalyst	Total TON	A/(K + L) ratio	Yield[a] (%)	Ref.
I	656	8.5[b]	58.7	11
II	858	7.7[b]	85.8	12
III	442	9.8	88.3	13
IV	622	8.7	62.2	14
V	601	7.1	60.1	15
VI	974	8.6	97.4	16
1	654	23.6	28.0	This work
2	589	22.4	25.2	This work
3	359	14.4	15.4	This work

[a] Yield based on *m*-CPBA concentration. [b] The ratio given is A/K.

observed with the present catalysts. The results suggest that the introduction of donor groups such as aniline, naphthylamine and benzylamine positively influences alcohol selectivity, but, does not enhance the overall yield.

The reaction when performed under an O_2 atmosphere (Table 5, entry 5) drastically reduced the product formation (TON, 143) and the A/(K + L) ratio (1.8), which could be attributed to the Russell termination of the radical chain reaction. During the oxidation process, the reactive species generate cyclohexyl radicals ($Cy^{6\bullet}$) by abstracting a hydrogen atom from cyclohexane. Upon exposure to O_2, $Cy^{6\bullet}$ radicals react with O_2 to form cyclohexyl peroxy radical species ($Cy_6OO^{\bullet}$). In the next step, radical coupling between two $Cy_6OO^{\bullet}$ species leads to the formation of $Cy_6OOOOCy_6$ tetroxide, and it eventually produces an equimolar amount of cyclohexanol and cyclohexanone. The formation of $Cy^{6\bullet}$ radicals during the oxidation process was further confirmed by performing the reaction in the presence of CBr_4 and identifying the presence of bromocyclohexane in the post-reaction mixture. This occurs due to the bromine atom abstraction from CBr_4 by $Cy^{6\bullet}$ radicals generated in the reaction (Fig. S11†).

Afterwards, the effect of the ring size in the oxidation reaction was studied using other cycloalkanes such as cyclopentane (Cy^5H), cycloheptane (Cy^7H) and cyclooctane (Cy^8H) in the presence of catalyst **1** and the results are provided in Table 7 (Fig. S12†). The obtained total TON and overall yield were correlated to the ring size of the substrates. For example, the total TON achieved was only 385 in the case of cyclopentane, whereas in the case of cyclooctane, it reached 834. Although the bond dissociation energy of cyclopentane (95.6 kcal mol^{-1}) is less than that of cyclohexane (99.5 kcal mol^{-1}), the latter was more susceptible to oxidation.[7] Similar observations were reported for nickel and cobalt catalysts using *m*-CPBA as the oxidant.[28,41]

The regioselectivity of reactive species was examined using catalyst **1** and substrates such as adamantane and methylcyclohexane with primary (1°), secondary (2°), and tertiary (3°) C–H bonds (Tables S1 and S2†). The oxidation of adamantane afforded 1-adamantanol (3°-ol), 2-adamantanol (2°-ol), 2-adamantanone (2°-one) and 1-chloroadamantane (3°-Cl) with a total TON of 337 and 3°/2° ratio of 8.6 (Table S1 and Fig. S12†). If the adamantane oxidation reaction proceeds *via* a Fenton-type mechanism ($^{\bullet}OH$ radical), a poor 3°/2° = 0.4–1.3 is typically observed.[29] A 3°/2° ratio in the range of 4.4–6.9 was reported by Hartwig *et al.* stating the involvement of 3-chlorobenzoyloxy radical in the catalytic cycle.[29] A much higher value in the range of 8.7–18.7 is noted in a few reports where the involvement of a nickel oxygen species was proposed.[4,16] Even though the ratio determined in the present study can be used to discard the possibility of the Fenton-type mechanism, it does not ensure or exclude the presence of 3-chlorobenzoyloxy radical or the nickel-based oxidant in the catalytic cycle. Further, the oxidation of methylcyclohexane was carried out using **1** and obtained tertiary (3°-ol), secondary (*o*, *m*, *p*-ols and 2°-ones) and primary (1°-ol) C–H oxidised products with a preference for secondary C–H oxidation (3°-ol : 2°-ols = 36 : 64). In contrast, the control experiment without any catalyst afforded 3°-ol majorly with poor overall yield (3°-ol : 2°-ols = 82 : 18) (Table S2†). Similar findings have been noted in previous studies where a nickel-based oxidant was proposed.[16,21]

Furthermore, to identify if any nickel intermediate is formed during the catalytic reaction, the reaction of catalyst **1** and *m*-CPBA was examined using UV-vis spectroscopy at room temperature. However, no spectral changes were noticed in the complex spectrum (5 mM) after the addition of *m*-CPBA (1 equiv.). Despite that, the addition of the base, triethylamine (1 equiv.) in the reaction mixture led to a redshift in the absorption bands of complex **1** from 551 to 561 nm, 762 to 771 nm, and 880 to 934 nm (Fig. S13a†). HRMS analysis of the reaction mixture revealed the formation of an *m*-CBA adduct of complex **1** (m/z = 545.0895 $[Ni(\mathbf{L1}) + (m\text{-CBA-H})]^+$ (calcd = 545.0890) (Fig. S13b†). In addition, the *m*-CBA adduct formation was further confirmed by the same spectral pattern obtained upon the reaction of **1** (5 mM) with *m*-CBA (1 equiv.) in the presence of triethylamine (1 equiv.) in acetonitrile at room temperature (Fig. S13a†).

Nevertheless, these observations do not conclusively substantiate the formation of *m*-CPBA or *m*-CBA adduct during the oxidation of cycloalkanes using catalysts **1–3**. In general, our results demonstrate that catalysts **1–3** are capable of catalysing the oxidation of a series of cycloalkanes using *m*-CPBA as the oxidant with excellent alcohol selectivity. By considering recent advances in the mechanistic studies of this chemistry, three possible pathways are proposed for the cycloalkane oxidation catalyzed by complexes **1–3** (Scheme 3). The high A/(K + L) ratio obtained and preferential oxidation of 2° C–H bonds in methylcyclohexane direct towards the contribution of nickel-based oxidants (paths 1 and 2). Although the reports in the last decade discussed a mechanism that occurs exclusively through path 1,[11,12,14,15,18–20] the latest theoretical and experimental findings validate the contribution of paths 2 and 3.[13,28–31] All the pathways are expected to start with the formation of an *m*-CPBA adduct from the reaction of the nickel(II) complex and *m*-CPBA. If

Table 7 Oxidation of cycloalkanes using **1**[a]

Substrate[b] (Cy^nH)	Cy^nCl (TON)	A (TON)	K (TON)	Total TON[c,d]	PhCl (TON)	Yield[e] (%)
Cy^5H	92	278	15	385	473	16.5
Cy^6H	136	497	10	654	878	28.0
Cy^7H	186	506	70	762	436	32.6
Cy^8H	228	532	74	834	380	35.7

[a] Cy^nCl = chloro derivative of the respective substrate, A = cycloalcohol, K = cycloketone, PhCl = chlorobenzene. [b] Reaction conditions: substrate (2.8 M), oxidant (0.35 M), catalyst (0.15 mM) in DCM : MeCN solvent mixture (v/v = 3 : 1), 60 °C, 2 h under N_2. [c] TON = number of mmol of product/number of mmol of catalyst. The TON is the average of three determinations. [d] TON of lactone is excluded. [e] Yield based on *m*-CPBA.

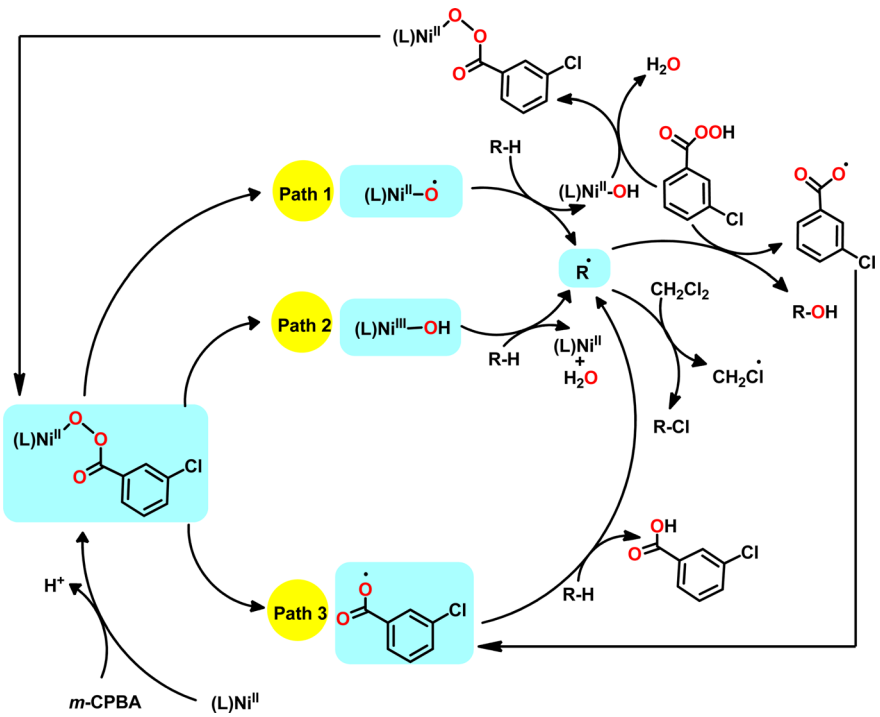

Scheme 3 Possible mechanistic pathways of cycloalkane oxidation catalysed by complexes **1–3** using *m*-CPBA as the oxidant.

the oxidation proceeds *via* path 1, the formed *m*-CPBA adduct undergoes O–O homolysis to generate [(L)Ni^{II}–O$^{\bullet}$] and this species further abstracts a hydrogen atom from the substrate to form R$^{\bullet}$ radical. In path 2, a hydroxo species [(L)Ni^{III}–OH] produced from the *m*-CPBA adduct is responsible for the generation of the substrate radical (R$^{\bullet}$). Unlike paths 1 and 2, a non-nickel-based reactive species (3-chlorobenzoyloxy radical) is involved in path 3 for the generation of R$^{\bullet}$ radicals. Nonetheless, in all the cases, the formed R$^{\bullet}$ radicals either react with *m*-CPBA to produce cyclic alcohol or abstract a chlorine atom from the dichloromethane solvent to produce chlorocyclohexane. Even though the literature provides evidence for the aryloxy radical mechanism, efforts to trap or characterise the proposed nickel-based oxidants have not yielded success to date.

4. Conclusion

Three monoamidate tetradentate ligands (**L1–L3**) and the respective nickel(II) complexes (**1–3**) were prepared and characterised. The catalytic potential of **1–3** was evaluated in the oxidation of cyclohexane using *m*-CPBA as the oxidant. Complexes showed activity in the order **1** (654) > **2** (589) > **3** (359) with a high A/(K + L) ratio up to 23.6. In addition, oxidation of other cycloalkanes such as cyclopentane, cycloheptane, cyclooctane, methylcyclohexane and adamantane was performed using catalyst **1**. Strikingly, the ring size of the substrates influenced the oxidation susceptibility of the substrates due to which cyclopentane oxidation resulted in low overall product yield and cyclooctane oxidation resulted in high overall product yield. A relatively high 3°/2° ratio (8.6) determined for adamantane oxidation confirmed the non-involvement of the Fenton-type mechanism (3°/2° = 0.4–1.3) in the catalytic cycle. Similarly, the preferential oxidation of 2° C–H bonds in methylcyclohexane indicated the possible participation of nickel-based oxidant in the oxidation reaction. However, the presence of chlorinated products and a high amount of chlorobenzene in the reaction mixture support the major contribution of the 3-chlorobenzoyloxy radical mechanism.

Data availability

The data that support the findings of the present study are available in the ESI† of this article. CCDC 2371833 (for **2**) and 2371834 (for **3**) contain the supplementary crystallographic data for this article.

Conflicts of interest

There are no conflicts to declare.

Acknowledgements

MS sincerely acknowledges the Department of Science and Technology for the award of the DST-Inspire Faculty Research Grant (IFA-17-CH286), the Science and Engineering Research Board (SERB) for the Core Research Grant (CRG/2023/002850) and the National Institute of Technology Calicut for the Faculty Research Grant (NIT/DEAN(R&C)/FRG/2018-19/3). A.R. acknowledges the UGC-SRF for the fellowship to pursue her PhD. We thank the CMC, NIT Calicut for NMR characterisations. S.M. acknowledges the Spain Ministry of Science (FJC2021-047874-I) for providing the fellowship to support his research work. We thank Prof. Miquel Costas, IQCC, Universitat

de Girona, Spain, for helping us to record mass spectra and single crystal X-ray data of the complexes.

References

1 B. Gabriele, *Molecules*, 2022, **27**, 1227.
2 V. P. Ananikov, L. L. Khemchyan, Yu. V. Ivanova, V. I. Bukhtiyarov, A. M. Sorokin, I. P. Prosvirin, S. Z. Vatsadze, A. V. Medved'ko, V. N. Nuriev, A. D. Dilman, V. V. Levin, I. V. Koptyug, K. V. Kovtunov, V. V. Zhivonitko, V. A. Likholobov, A. V. Romanenko, P. A. Simonov, V. G. Nenajdenko, O. I. Shmatova, V. M. Muzalevskiy, M. S. Nechaev, A. F. Asachenko, O. S. Morozov, P. B. Dzhevakov, S. N. Osipov, D. V. Vorobyeva, M. A. Topchiy, M. A. Zotova, S. A. Ponomarenko, O. V. Borshchev, Yu. N. Luponosov, A. A. Rempel, A. A Valeeva, A. Yu. Stakheev, O. V. Turova, I. S. Mashkovsky, S. V. Sysolyatin, V. V. Malykhin, G. A. Bukhtiyarova, A. O. Terent'ev and I. B. Krylov, *Russ. Chem. Rev.*, 2014, **83**(10), 885–985.
3 T. Punniyamurthy, S. Velusamy and J. Iqbal, *Chem. Rev.*, 2005, **105**, 2329–2363.
4 M. Sankaralingam, M. Balamurugan and M. Palaniandavar, *Coord. Chem. Rev.*, 2020, **403**, 213085.
5 A. Rajeev, M. Balamurugan and M. Sankaralingam, *ACS Catal.*, 2022, **12**, 9953–9982.
6 M. T. Musser and E. I. Du, *Cyclohexanol and Cyclohexanone, Ullmann's Encycl. Ind. Chem.*, 2012, pp. 49–60.
7 Y.-R. Luo, *Handbook of Bond Dissociation Energies in Organic Compounds*, CRC Press, 1st edn, 2002.
8 U. Schuchardt, R. Pereira and M. Rufo, *J. Mol. Catal. A: Chem.*, 1998, **135**, 257–262.
9 A. R. Silva, T. Mourão and J. Rocha, *Catal. Today*, 2013, **203**, 81–86.
10 N. M. F. Carvalho, A. Horn and O. A. C. Antunes, *Appl. Catal., A*, 2006, **305**, 140–145.
11 T. Nagataki, Y. Tachia and S. Itoh, *Chem. Commun.*, 2006, 4016–4018.
12 T. Nagataki and S. Itoh, *Chem. Lett.*, 2007, **36**, 748–749.
13 T. Wada, H. Sugimoto, Y. Morimoto and S. Itoh, *Polyhedron*, 2022, **227**, 116150.
14 M. Balamurugan, R. Mayilmurugan, E. Suresh and M. Palaniandavar, *Dalton Trans.*, 2011, **40**, 9413–9424.
15 M. Sankaralingam, P. Vadivelu and M. Palaniandavar, *Dalton Trans.*, 2017, **46**, 7181–7193.
16 I. Terao, S. Horii, J. Nakazawa, M. Okamura and S. Hikichi, *Dalton Trans.*, 2020, **49**, 6108–6118.
17 A. Rajeev and M. Sankaralingam, Highlights of Oxygen Atom Transfer Reactions Catalysed by Nickel Complexes, *Oxygen Atom Transfer Reactions*, Mechanisms of oxidation reactions, Bentham Science., 2023, pp. 62–90.
18 T. Nagataki, K. Ishii, Y. Tachi and S. Itoh, *Dalton Trans.*, 2007, 1120–1128.
19 M. Sankaralingam, M. Balamurugan, M. Palaniandavar, P. Vadivelu and C. H. Suresh, *Chem. - Eur. J.*, 2014, **20**, 11346–11361.
20 M. Sankaralingam, P. Vadivelu, E. Suresh and M. Palaniandavar, *Inorg. Chim. Acta*, 2013, **407**, 98–107.
21 S. Hikichi, K. Hanaue, T. Fujimura, H. Okuda, J. Nakazawa, Y. Ohzu, C. Kobayashi and M. Akita, *Dalton Trans.*, 2013, **42**, 3346–3356.
22 P. Pirovano, E. R. Farquhar, M. Swart and A. R. McDonald, *J. Am. Chem. Soc.*, 2016, **138**, 14362–14370.
23 P. Pirovano, B. Twamley and A. R. McDonald, *Chem. - Eur. J.*, 2018, **24**, 5238–5245.
24 P. Pirovano, A. R. Berry, M. Swart and A. R. McDonald, *Dalton Trans.*, 2018, **47**, 246–250.
25 T. Corona, F. F. Pfaff, F. AcuÇa-ParØs, A. Draksharapu, C. J. Whiteoak, V. Martin-Diaconescu, J. Lloret-Fillol, W. R. Browne, K. Ray and A. Company, *Chem. - Eur. J.*, 2015, **21**, 15029–15038.
26 T. Corona, A. Draksharapu, S. K. Padamati, I. Gamba, V. Martin-Diaconescu, F. Acuña-Pares, W. R. Browne and A. Company, *J. Am. Chem. Soc.*, 2016, **138**, 12987–12996.
27 A. Juvanteny, C. Souilah, R. Quintero, C. García-Bellido, N. Pagès-Vilà, T. Corona, P. Salvador and A. Company, *Inorg. Chem.*, 2024, **63**, 14325–14334.
28 A. Rajeev, A. T. Thomas, A. Das and M. Sankaralingam, *Eur. J. Inorg. Chem.*, 2024, **27**, e202400205.
29 Y. Qiu and J. F. Hartwig, *J. Am. Chem. Soc.*, 2020, **142**, 19239–19248.
30 T. Shinke, M. Itoh, T. Wada, Y. Morimoto, S. Yanagisawa, H. Sugimoto, M. Kubo and S. Itoh, *Chem. - Eur. J.*, 2021, **27**, 14730–14737.
31 Z. Wu, D. Sun, Y. Lee, Y. Zhao, W. Nam and Y. Wang, *Dalton Trans.*, 2023, **52**, 8676–8684.
32 L. Falivene, Z. Cao, A. Petta, L. Serra, A. Poater, R. Oliva, V. Scarano and L. Cavallo, *Nat. Chem.*, 2019, **11**, 872–879.
33 A. Das, A. Rajeev, S. Bhunia, M. Arunkumar, N. Chari and M. Sankaralingam, *Inorg. Chim. Acta*, 2021, **526**, 120515.
34 L. Zhang, S. Li, H. Liu, Y. Cheng, X. Wei, X. Chai and G. Yuan, *Inorg. Chem.*, 2020, **59**(23), 17464–17472.
35 L. Ma, S. Li, H. Zheng, J. Chen, L. Lin, X. Ye, Z. Chen, Q. Xu, T. Chen, J. Yang, N. Qiu, G. Wang, A. Peng, Y. Ding, Y. Wei and L. Chen, *Eur. J. Med. Chem.*, 2011, **46**, 2003–2010.
36 H. G. Lee, J. H. Lee, S. P. Jang, I. H. Hwang, S. Kim, Y. Kim, C. Kim and R. G. Harrison, *Inorg. Chim. Acta*, 2013, **394**, 542–551.
37 A. P. Singh, N. K. Kaushik, K. Verma and R. Gupta, *Indian J. Chem.*, 2011, **50**(1), 474–483.
38 A. E. Wickenden and R. A. Krause, *Inorg. Chem.*, 1965, **4**, 404–407.
39 H. D. Lutz, R. A. Becker and W. Eckers, *Indian J. Chem.*, 1983, **39**, 7–14.
40 K. H. Bok, M. M. Lee, G. R. You, H. M. Ahn, K. Y. Ryu, S. Kim, Y. Kim and C. Kim, *Chem. - Eur. J.*, 2017, **23**, 3117–3125.
41 Y. Morimoto, Y. Shimaoka, K. Fukui and S. Itoh, *ACS Omega*, 2024, **9**(22), 23624–23633.